Residual currents
Numerical model
Bristol Channel
Severn Estuary

Courants résiduels
Modèle numérique
Canal de Bristol
Estuaire du Severn

Computed and observed residual currents in the Bristol Channel

R. J. Uncles

Natural Environment Research Council, Institute for Marine Environmental Research, Prospect Place, The Hoe, Plymouth, England.

Received 2/2/81, in revised form 20/8/81, accepted 12/9/81.

ABSTRACT

A depth averaged numerical model is used to evaluate the residual currents generated by horizontal density gradients and M_2 tidal non-linearities in the Bristol Channel (UK), a simple linear theory is used to investigate the mechanisms responsible for generation of residual currents, and computed data are compared with observations.
Current patterns are presented for flows resulting from non-linearities in the continuity equation, and for those due to density gradients, advection non-linearities and friction non linearities in the momentum equation. The comparison of computed with observed currents shows qualitative similarities at most of the stations, and reasonable agreement for those stations where observations were carried out over one month, and where allowance is made for the expected depth variations due to density gradients.

Oceanol. Acta, 1982, **5**, 1, 11-20.

RÉSUMÉ

Courants résiduels calculés et observés dans le canal de Bristol.

Un modèle numérique du courant moyen intégré sur la verticale est utilisé pour évaluer les courants résiduels produits par les gradients de densité horizontaux et les non-linéarités de la marée M_2 dans le canal de Bristol. Au moyen d'une théorie linéaire simple, on étudie les mécanismes qui produisent les courants résiduels. Les résultats du calcul sont comparés avec des observations.
Les débits provenant des non-linéarités dans l'équation de continuité et ceux causés par les gradients de densité, les non-linéarités d'advection et les non-linéarités de friction dans l'équation de la force vive sont présentés au moyen de cartes des courants. A la plupart des stations, on note, en les comparant, des similarités qualitatives entre les courants calculés et observés. Leur accord est très acceptable aux stations où les observations étaient réalisées sur un mois et où on tient compte des variations attendues de la profondeur, causées par les gradients de densité.

Oceanol. Acta, 1982, **5**, 1, 11-20.

This work is dedicated to the memory of Clare Hawke, who prepared the diagrams for the paper.

INTRODUCTION

This paper is concerned with the application of a two-dimensional, hydrodynamical model to the calculation of depth averaged density-driven and tidally-induced residual currents in the Bristol Channel and Severn Estuary, and with the comparison of these currents with observed data. Figure 1 *a* shows mean depths, *h*, over the region, and the positions at which residual currents have been measured (Uncles, Jordan, in prep.). The tidal range is large, and whilst the associated strong tidal currents ensure that the water column is vertically homogeneous for temperature and salinity, the horizontal gradients in salinity due to freshwater inputs (see Fig. 1 *b*) can have a significant effect on the vertical profile of residual current.

The distribution of M_2 ellipse semi-major axis (the maximum flood or ebb current) is shown in Figure 1 *c*; over most of the region the ellipticity is small, so that at each point the tidal currents are very nearly parallel or antiparallel to a given straight line, and are essentially coincident with the centre axis of the channel, or locally parallel to coastlines. These large tidal currents generate both a significant Stokes drift, see Figure 1 *d*, and a tidally-induced residual current (Nihoul, Ronday, 1975; Tee, 1976; 1977; Prandle, 1978; Pingree, Maddock, 1977; Pingree, 1978; Yanagi, 1976; 1977; 1978; Oonishi, 1977; 1978; Uncles, Jordan, 1980; Zimmerman, 1978).

Individual contributions to the residual current are investigated here from a rather qualitative stance, in order to understand how each mechanism for non-linear generation produces a current, and to compare these currents with those driven by density gradients. Computed data on depth averaged residual currents for the Bristol Channel have recently been reported by Owen (1980), and the present work may be considered an extension of Owen's analysis in which individual mechanisms are investigated, density effects are incorporated, and comparisons are made with observed data.

EQUATIONS AND METHODS

Numerical model

The depth averaged equations of continuity and momentum are, respectively:

$$\frac{\partial \zeta}{\partial t} = -\nabla.(\mathrm{H}\,\mathbf{v}) \tag{1}$$

and:

$$\frac{\partial \mathbf{v}}{\partial t} = -(\mathbf{v}.\nabla)\mathbf{v} - g\nabla\zeta - \mathbf{f}\times\mathbf{v}$$

$$\frac{-\mathrm{D}\,\mathbf{v}\,|\mathbf{v}|}{\mathrm{H}} - \frac{1}{2}g\,\mathrm{H}\nabla\ln\rho + \mathrm{N}\nabla^2\mathbf{v}, \tag{2}$$

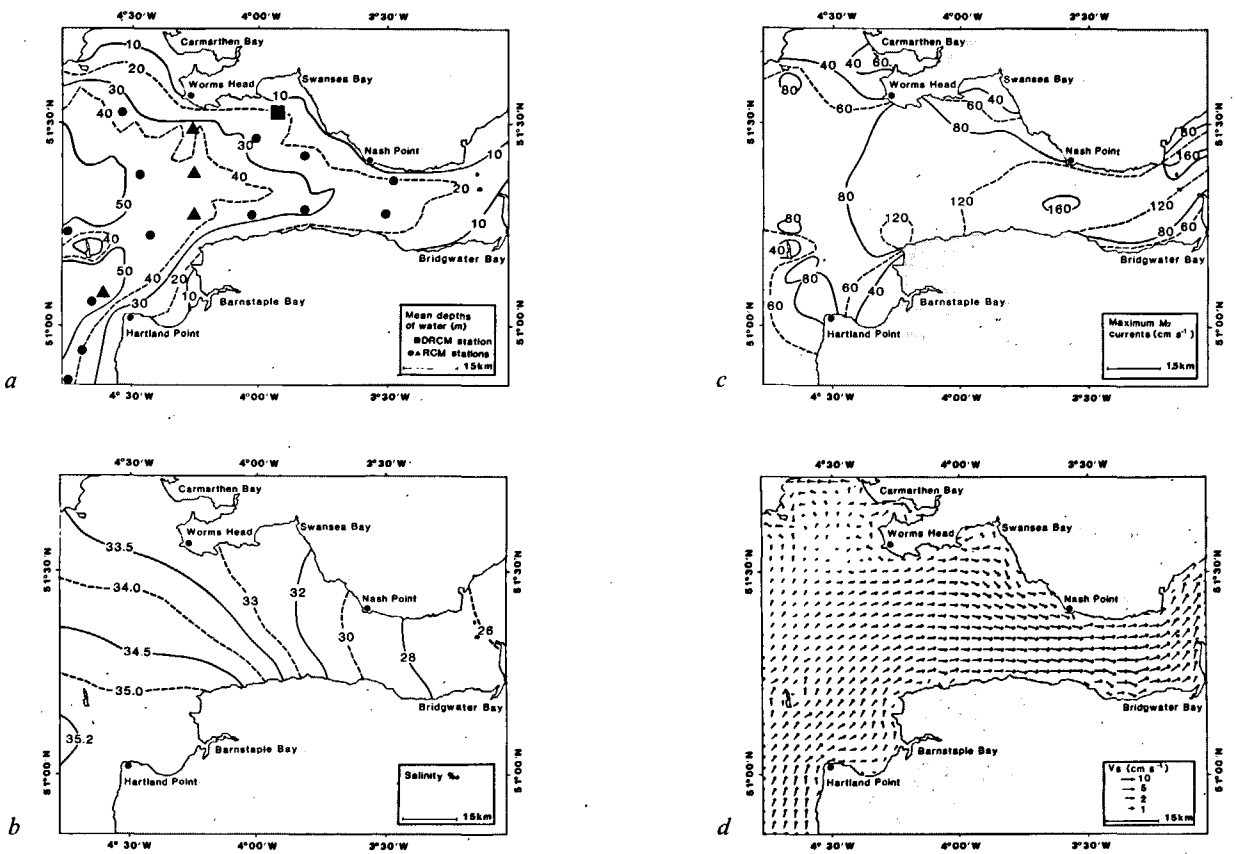

Figure 1

Characteristic properties of the Bristol Channel. The region up-channel of Nash Point is the Severn Estuary; between Worms Head and Nash Point is the eastern Bristol Channel, and down-channel of Worms Head is the western Bristol Channel. (a) Mean depths of water, h, and location of current meter stations. ● and ▲ denote stations at which moored recording current meters (RCMs) *were deployed over a few tidal cycles and one month respectively;* ■ *denotes station* D, *where a direct reading current meter* (DRCM) *was deployed for five tidal cycles. (b) Typical distribution of salinity,* $S(^0/_{00})$. *(c) Distribution of maximum* M_2 *tidal currents,* E_{M_2} *(cm.sec.*$^{-1}$*). (d) Stokes drift,* v_S, *generated by* M_2 *tides (speeds drawn on a logarithmic scale).*

in which meteorological effects are ignored, and where ζ is surface elevation, $\mathbf{v}$ the velocity, H the total depth of water $(h+\zeta)$, ρ the density of seawater, $\mathbf{f}$ the Coriolis parameter, g the acceleration due to gravity, D the friction parameter (2.5×10^{-3}), and N the coefficient of horizontal eddy viscosity (10^6 cm^2.sec.$^{-1}$); also:

$$\mathbf{v}=(u, v, 0), \qquad \mathbf{f}=(0, 0, f)$$

and:

$$\nabla=(\partial/\partial x, \partial/\partial y, 0).$$

The density gradients can be related to the salinity distribution, S (Bowden, Hamilton, 1975):

$$\nabla \ln \rho \cong a \nabla S \qquad \text{with} \quad a=7.8\times10^{-4}.$$

Subsequent calculations use the distribution of S shown in Figure 1 *b* in order to compute density gradients.

Equations (1) and (2) are solved in finite-difference form using a 53×43 array of points with spacing $(3.1\times3.1$ km) to cover the region (2°37.0′W-4°58.4′W, 50°32.5′N-51°45.8′N). The modelled region is larger than that for which results are presented (see Fig. 1 *a* to *d*), and extends further to the west by five lattice points, and to the south by nine; this avoids the presentation of possible spurious circulations at the open boundary (see, for example, Prandle, 1978, p. 198). Similarly, results are not presented for the eastern Severn Estuary, where spatial resolution is poor. The numerical methodology is essentially that described by Flather and Heaps (1975). Seaward boundary conditions on the elevations consist of data for the residual, and for the M_2 and M_4 tides. These data were obtained by interpolating results from a model of the southwest shelf having a lattice spacing of about 15 km on the shelf, decreasing to about 7 km in the Bristol Channel (Miles, 1979, p. 79).

Generation of residual currents

Averaging equations (1) and (2) over an M_2 tidal period gives:

$$\frac{\partial \langle \zeta \rangle}{\partial t} + \nabla.(h \langle \mathbf{v} \rangle) = -\nabla.\langle \zeta \mathbf{v} \rangle \tag{3}$$

and:

$$\frac{\partial \langle \mathbf{v} \rangle}{\partial t} + g\nabla\langle\zeta\rangle + \mathbf{f}\times\langle\mathbf{v}\rangle - N\nabla^2\langle\mathbf{v}\rangle = -\langle(\mathbf{v}.\nabla)\mathbf{v}\rangle - \left\langle\frac{D\mathbf{v}|\mathbf{v}|}{H}\right\rangle - \frac{1}{2}gha\nabla S. \tag{4}$$

In this region the residual and overtide currents and elevations are much smaller than the semidiurnal currents and elevations; for M_2 tides and overtides it follows that:

$$\zeta=\langle\zeta\rangle+\zeta_{M_2}+\zeta_{M_4}+\ldots,$$

with:

$$|\zeta_{M_2}| \gg |\langle\zeta\rangle|, \quad |\zeta_{M_4}|, \quad \ldots$$

and:

$$\mathbf{v}=\langle\mathbf{v}\rangle+\mathbf{v}_{M_2}+\mathbf{v}_{M_4}+\ldots,$$

with:

$$|\mathbf{v}_{M_2}| \gg |\langle\mathbf{v}\rangle|, \quad |\mathbf{v}_{M_4}|, \quad \ldots$$

The Stokes drift, given by $\langle(\mathbf{v}-\langle\mathbf{v}\rangle)(\zeta-\langle\zeta\rangle)\rangle/h$ (Tee, 1976; Uncles, Jordan, 1980) and shown in Figure 1 *d*, can therefore be written to first-order accuracy as:

$$\mathbf{v}_S=(u_S, v_S)=\langle\zeta_{M_2}\mathbf{v}_{M_2}\rangle/h. \tag{5}$$

Using this definition, the linearization of equation (3) gives:

$$\frac{\partial\langle\zeta\rangle}{\partial t}+\nabla.(h\langle\mathbf{v}\rangle)=-\nabla.(h\mathbf{v}_S), \tag{6}$$

Equation (4) may also be linearized, but in this case it is sufficiently precise for a qualitative understanding to consider that the directions of the semidiurnal and overtide currents are coincident straight lines; taking local co-ordinate axes (x, y) such that x is parallel to the flood tidal currents, $\mathbf{v}=(u, 0, 0)$ at $x=y=0$, and neglecting M_8 and higher overtides, then the linearization gives (for methodology see, for example, Heaps, 1978; Hunter, 1975 and 1979):

$$\psi^{(u)} \equiv \frac{\partial\langle u\rangle}{\partial t}+g\frac{\partial\langle\zeta\rangle}{\partial x} - f\langle v\rangle - N\nabla^2\langle u\rangle + \frac{4DE_{M_2}}{\pi h}\langle u\rangle = -\frac{1}{4}\frac{\partial}{\partial x}(E_{M_2}^2) - \frac{4DE_{M_2}}{3\pi h}.[E_{M_4}\cos\varphi_e - 2u_S] - \frac{1}{2}gah\frac{\partial S}{\partial x} \tag{7}$$

and:

$$\psi^{(v)} \equiv \frac{\partial\langle v\rangle}{\partial t}+g\frac{\partial\langle\zeta\rangle}{\partial y}+f\langle u\rangle - N\nabla^2\langle v\rangle + 2\frac{DE_{M_2}}{\pi h}\langle v\rangle = E_{M_2}^2/2R - \frac{1}{2}gah\frac{\partial S}{\partial y}, \tag{8}$$

where:

$$u_{M_2}=E_{M_2}\cos(\omega_{M_2}t-e_{M_2}),$$
$$u_{M_4}=E_{M_4}\cos(\omega_{M_4}t-e_{M_4}),$$
$$\varphi_e=2e_{M_2}-e_{M_4},$$

and where R is the local radius of curvature of the M_2 currents ($R=-dx/d\Phi$ evaluated at $x=0=\Phi$, where Φ is the angle between the M_2 flood current and the positive x direction).

Assuming steady-state conditions in equations (6) to (8) it is possible to identify currents and elevations due to density gradients ($\mathbf{v}_D$, ζ_D), non-linear advection ($\mathbf{v}_A$, ζ_A), friction ($\mathbf{v}_F$, ζ_F) and continuity ($\mathbf{v}_C$, ζ_C); the sum of currents is the Eulerian residual, $\mathbf{v}_E$:

$$\langle \mathbf{v} \rangle = \mathbf{v}_E = \mathbf{v}_D + \mathbf{v}_A + \mathbf{v}_F + \mathbf{v}_C, \tag{9}$$

also:

$$\langle \zeta \rangle = \zeta_E = \zeta_D + \zeta_A + \zeta_F + \zeta_C. \tag{10}$$

In local co-ordinates the linearized governing equations are [with, for example, $\psi_D^{(u)} \equiv \psi^{(u)}(\mathbf{v}_D, \zeta_D)$]:

$$\left.\begin{aligned} &\nabla.(h\,\mathbf{v}_D) = 0, \qquad \psi_D^{(u)} = -\frac{1}{2} gah \frac{\partial S}{\partial x}, \\ &\psi_D^{(v)} = -\frac{1}{2} gah \frac{\partial S}{\partial y}, \end{aligned}\right\} \tag{11}$$

$$\left.\begin{aligned} &\nabla.(h\,\mathbf{v}_A) = 0, \qquad \psi_A^{(u)} = -\frac{1}{4} \frac{\partial}{\partial x}(E_{M_2}^2), \\ &\psi_A^{(v)} = E_{M_2}^2 / 2\,R, \end{aligned}\right\} \tag{12}$$

$$\left.\begin{aligned} &\nabla.(h\,\mathbf{v}_F) = 0, \qquad \psi_F^{(u)} = \frac{4\,DE_{M_2}}{3\pi h}[2u_S - E_{M_4}\cos\varphi_e], \\ &\psi_F^{(v)} = 0 \end{aligned}\right\} \tag{13}$$

and:

$$\left.\begin{aligned} &\nabla.(h\,\mathbf{v}_C) = -\nabla.(h\,\mathbf{v}_S), \qquad \psi_C^{(u)} = 0, \\ &\psi_C^{(v)} = 0. \end{aligned}\right\} \tag{14}$$

Evaluation of residual currents

Eulerian residual currents, $\mathbf{v}_E$ [equation (9)], are derived from equations (1) and (2) by averaging computed velocities over a tidal cycle; the seaward boundary conditions on ζ_E [equation (10)] comprise estimated values for ζ_D, together with interpolated values of the tidal residual ($\zeta_A + \zeta_F + \zeta_C$) from a coarse-grid tidal model of the southwest shelf (Miles, 1979). The sensitivity of these solutions to the assumed boundary conditions is discussed in the Appendix.

M_2 currents and elevations are not significantly affected by either density gradients or advection processes (and nor, therefore, are $\mathbf{v}_S$, $\psi^{(u)}$ and $\psi^{(v)}$ in equations (5) to (8), and the source terms in equations (11) and (12)); it follows that both $\mathbf{v}_D$ and $\mathbf{v}_A$ can be computed from equations (1) and (2) by solving them with and without the appropriate source terms [$(\mathbf{v}.\nabla)\,\mathbf{v}$ or $(1/2)\,g\,H\,\nabla \ln \rho$] and their associated boundary conditions (see later), and subtracting the residual currents and elevations computed without the source term from those computed with the source term.

The residual elevations and currents generated by continuity non-linearities, ($\mathbf{v}_C$, ζ_C), can be computed by omitting advection and density gradients from equation (2), and linearizing the friction term; the linearization used here is very crude, and employs a friction coefficient which is the average of those applicable to transverse and parallel residual currents [see equations (7) and (8)].

The residual elevations and currents generated by non-linear frictional forces ($\mathbf{v}_F$, ζ_F) can be computed from equations (1) and (2) by omitting advection and density gradient forcing from equation (2), and linearizing equation (1) by replacing the total depth, H, with h; this procedure is again approximate, and yields only an indication of ($\mathbf{v}_F$, ζ_F) because they depend on the amplitudes and phases of the M_4 currents (through E_{M_4} and φ_e in equation (13)), which are affected not only by seaward boundary conditions on the vertical M_4 tide, but also by non-linear processes which have been omitted from equations (1) and (2)—especially those contained in the continuity equation (Uncles, 1981). Nevertheless, it can be shown that the procedure used here is reasonable for qualitative results in the Bristol Channel.

Although computed values of $\mathbf{v}_C$ and $\mathbf{v}_F$ are in error due to approximations in the linearization of friction, and the linearization of continuity, respectively, solutions ($\mathbf{v}_C + \mathbf{v}_F$) can be computed which suffer from neither of these defects, and which are derived from equations (1) and (2) by omitting advection and density gradients from equation (2).

RESULTS

The magnitudes of the currents described by equations (11)-(14) are summarized in the Table for the western and eastern Bristol Channel, and for the Severn Estuary. Data are presented as averages and standard deviations for each region. The Table shows that $\mathbf{v}_A$ is dominant over the whole region, and is followed in magnitude by $\mathbf{v}_C$ and $\mathbf{v}_D$; $\mathbf{v}_F$ is exceedingly small.

Table

Averages and standard deviations of residual current speeds due to density gradients and various non-linear mechanisms over the western Bristol Channel (WBC), eastern Bristol Channel (EBC) and Severn (S).

WBC	EBC	S	$\lvert\langle \mathbf{v} \rangle\rvert$
	(mm.sec.$^{-1}$)		
40±42	31±22	51±39	$\mathbf{v}_E$
38±43	29±24	42±35	$\mathbf{v}_A$
8± 5	12± 7	5± 3	$\mathbf{v}_D$
4± 3	13± 6	28±16	$\mathbf{v}_C$
2± 2	4± 3	6± 5	$\mathbf{v}_F$
6± 4	14± 7	28±17	$(\mathbf{v}_C + \mathbf{v}_F)$

Currents $\mathbf{v}_C$ in the Table decrease towards the west because of decreasing values of $\mathbf{v}_S$ associated with smaller M_2 tidal elevations and currents, and the deeper water [see equations (5) and (14)], and these same causes also result in smaller values of $\mathbf{v}_F$ [see equations (13)]. Density currents $\mathbf{v}_D$ do not show a trend with position because the forcing term in equation (11) is proportional to $h\,\nabla S$, and although the depths, h, increase seawards the salinity gradients, ∇S, decrease. Similarly, the currents $\mathbf{v}_A$ do not show a trend because their magnitudes depend not only on the M_2 currents, but also on topographical irregularities [small R and large $\partial/\partial x$ in equation (12), see Zimmerman, 1978] which are not a systematic function of position.

Once generated, the residual currents are governed by the linearized dynamics described by $\psi^{(u)}$ and $\psi^{(v)}$ in

equations (7) and (8); the relative magnitudes of friction, Coriolis forces and eddy viscosity can be estimated as:

$$\frac{4\,DE_{M_2}}{\pi hf} \sim 1 \quad \text{and} \quad \frac{N\nabla^2\langle v\rangle}{f\langle v\rangle} \sim \frac{N}{f(\Delta s)^2} \sim 0.1,$$

using $\cong D = 2.5\times10^{-3}$, $\cong f = 1.14\times10^{-4}$ sec.$^{-1}$, $E_{M_2} \equiv 1$ m.sec.$^{-1}$ and $h \equiv 30$ m, and using the minimum length scale of $\Delta s = 3.1$ km in order to give a maximum weighting to the effects of viscosity. This analysis shows that the effects of friction and the Earth's rotation on the behaviour of the residual currents are comparable over the region, and that viscosity is negligible.

The residual currents, v_E, computed from equations (1) and (2) are plotted in Figure 2*a*, and the residual set-up of water level, ζ_E, in Figure 2*b*; this solution can be attributed to both density currents and the currents generated by non-linearities in the tidal dynamics, although v_E is very similar to that derived by Owen (1980), who ignored density effects. Individual components of the solution are considered in the following sections.

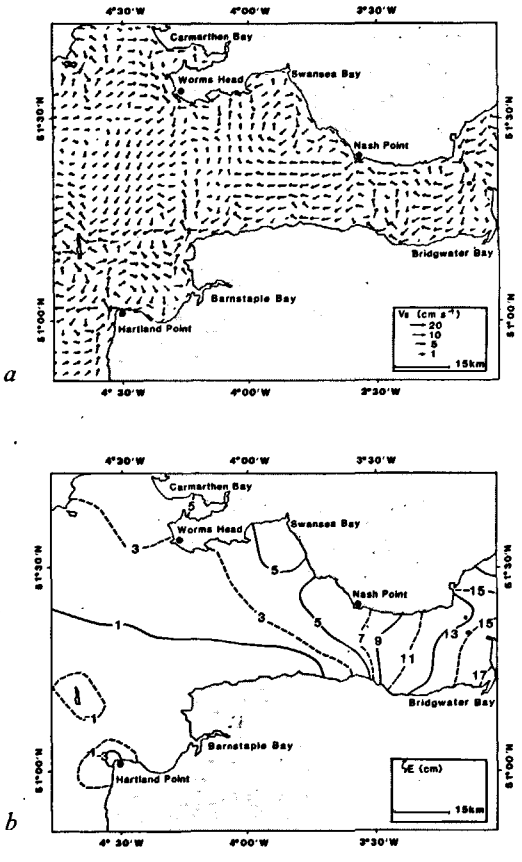

Figure 2
Residual currents and elevations for density and non-linear tidal effects. (a) v_E (speeds drawn on a logarithmic scale). (b) ζ_E (cm).

Density currents

Currents v_D, are shown in Figure 3*a* and the associated set-up, ζ_D, in Figure 3*b*. Contours for ζ_D resemble those for salinity, S (see Fig. 1*b*), and the surface slopes

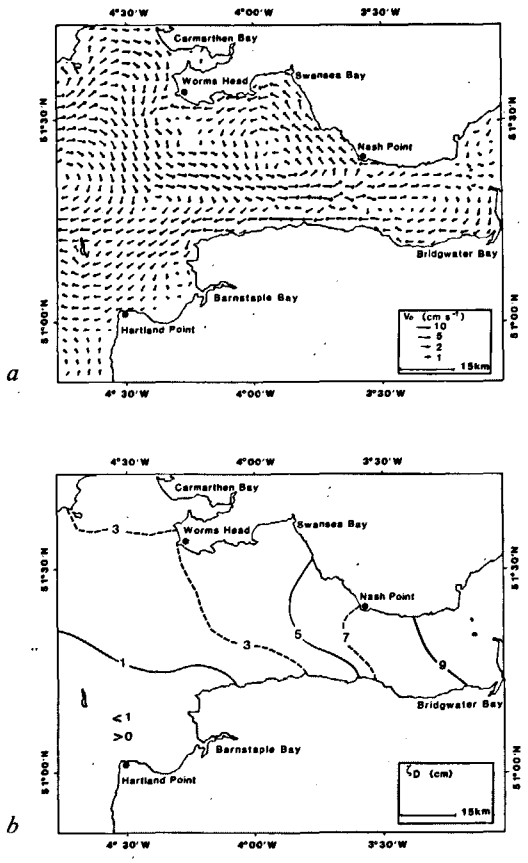

Figure 3
Density-driven residual currents and elevations. (a) v_D (speeds drawn on a logarithmic scale). (b) ζ_D (cm).

approximately balance the density gradient forcing, as expected for a partially enclosed channel. Because the density gradient forcing is generally largest in the deeper sections of the channel, the residual currents tend to flow into the channel through these sections and, driven by surface slopes, return seawards over the shallower regions, as shown in Figure 3*a*.

In the eastern Bristol Channel a typical value of the forcing is, from Figure 1*b*:

$$-\frac{1}{2}agh\frac{\partial S}{\partial x} \cong 1\times10^{-3}\ \text{cm.sec.}^{-2},$$

whereas from Figure 3*b*:

$$g\frac{\partial \zeta_D}{\partial x} \cong 1\times10^{-3}\ \text{cm.sec.}^{-2}.$$

A typical velocity, v_D (see Table) is 1.2 cm.sec.$^{-1}$ so that:

$$fv_D \sim \frac{4\,DE_{M_2}}{\pi h}.u_D \sim 1\times10^{-4}\ \text{cm.sec.}^{-2} \ll g\frac{\partial \zeta_D}{\partial x},$$

which emphasizes the near balance between surface slopes and density forcing. This result was used to estimate seaward boundary conditions on ζ_D, the surface slopes along the boundary being chosen to balance exactly the parallel component of density gradient forcing (see Appendix).

Advection currents

Currents, $\mathbf{v}_A$, and surface set-up, ζ_A, are plotted in Figures 4 *a* and *b* respectively. As with density currents, surface slopes must almost balance the forcing mechanisms in equation (12), with only small resultant forces available for driving currents. The M_2 tidal streams are essentially oriented along the channel axis, which can therefore be associated with the "x" direction in equation (12) for a study of the axial balance of forces, which is, neglecting eddy viscosity:

$$\psi_A^{(u)} = g\frac{\partial \zeta_A}{\partial x} - fv_A + \frac{4\,DE_{M_2}}{\pi h}.u_A = -\frac{1}{4}\frac{\partial}{\partial x}(E_{M_2}^2).$$

E_{M_2} increases from about 60 cm.sec.$^{-1}$ at the seaward boundary to about 160 cm.sec.$^{-1}$ in the mouth of the Severn (see Fig. 1 *c*), so that the axial advective forcing is down-channel; as a first approximation the axial change in water level is given by:

$$g\frac{\partial \zeta_A}{\partial x} \cong -\frac{1}{4}\frac{\partial}{\partial x}(E_{M_2}^2).$$

Thus, between the seaward boundary and the mouth of the Severn the lowering of sea-level is:

$$\delta\zeta_A \cong -\frac{1}{4g}.\delta(E_{M_2}^2) \cong -6\text{ cm},$$

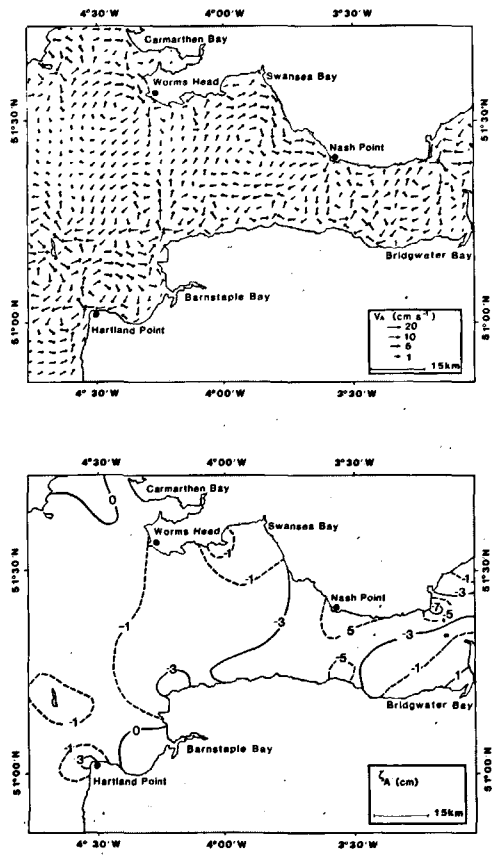

Figure 4

Advection-driven residual currents and elevations. (a) $\mathbf{v}_A$ *(speeds drawn on a logarithmic scale). (b)* ζ_A *(cm).*

which is close to the modelled value of −5 cm shown in Figure 4 *b*; on the assumption that transverse currents are prevented by transverse surface slopes, then the difference between these estimates is the surface elevation available for driving down-channel currents of magnitude:

$$u_A \cong \left[-\frac{1}{4}\frac{\partial}{\partial x}(E_{M_2}^2) - g\frac{\partial \zeta_A}{\partial x}\right] \cdot \frac{\pi h}{4\,DE_{M_2}} \cong -1\text{ cm.sec.}^{-1}.$$

The compensating return flows into the channel must occur in regions possessing low, or even negative gradients in tidal energy (such as can occur in bays). This mechanism is thought to be partially responsible for the seaward flows which occur in the southern part of the eastern Bristol Channel and the central part of the western Bristol Channel in Figure 4 *a*.

Superimposed on the gradual up-channel lowering of water level shown in Figure 4 *b* are transverse variations which show raised levels in bays and depressions off headlands. These gradients in sea level are essentially perpendicular to the tidal streams and can be described using the "y" component of motion given by equation (12), which is, omitting eddy viscosity:

$$\psi_A^{(v)} = g\frac{\partial \zeta_A}{\partial y} + fu_A + \frac{2\,DE_{M_2}}{\pi h}.v_A = E_{M_2}^2/2\,R.$$

Off a headland, R is small, E_{M_2} is large (see Fig. 1 *c*), and the large centrifugal forces drive residual currents "radially" away from the headland (these being fed by coastal currents converging on the headland), thereby producing a set-down in water level, as shown in Figure 4 *b*, [see Pingree (1978) for a discussion of headland effects]. Similarly, the centrifugal forcing of tidal streams as they follow the meandering axis of the channel, or curve around bays, leads to the generation of transverse residual flows and variations in water level. If the transverse set-up in the eastern Bristol Channel is considered, then in this region the flood tidal streams generally curve in an anticyclonic sense, with a radius of curvature (R) of about 80 km (based on the shape of the medial axis); with $E_{M_2} \cong 1$ m.sec.$^{-1}$ it follows that:

$$\frac{E_{M_2}^2}{2\,R} \cong 6\times10^{-4}\text{ cm.sec.}^{-2},$$

whereas the observed rise in water level between south and north coastlines gives:

$$g\frac{\partial \zeta_A}{\partial y} \cong 7\times10^{-4}\text{ cm.sec.}^{-2} \sim \frac{E_{M_2}^2}{2\,R},$$

so that an approximate balance exists; nevertheless, residual currents are driven from south to north where the centrifugal forces are strong and to the north, and the return flows occur in regions where the forces are small or reversed. In conjunction with the currents driven by axial gradients of tidal energy – which flow down-channel in the south of the region, this mechanism is thought to

account for the anticyclonic residual circulation in the eastern Bristol Channel shown in Figure 4*a*. It is also thought to partly account for the characteristic current patterns in Barnstaple and Carmarthen Bay, where residual currents flow into the central parts of each bay and return to sea as oppositely flowing coastal currents, although such flows will also result from headland effects at either end of each bay.

The seaward boundary conditions on ζ_A (see Appendix) are taken to be $(\zeta_E-\zeta_D)$, which is equivalent to assuming that boundary elevations for ζ_C and ζ_F are negligibly small; whilst this cannot be strictly valid, it is consistent with the small values of $\mathbf{v}_C$ and $\mathbf{v}_F$ shown in the Table for the western Bristol Channel.

Continuity and frictional currents

The methods used, and the errors involved, in computing $\mathbf{v}_C$ and $\mathbf{v}_F$ separately have already been mentioned. The computed data for $\mathbf{v}_C$ in Figure 5*a*, and for $\mathbf{v}_F$ in Figure 5*b*, must therefore be considered rather qualitative, indicating general features and magnitudes rather than precise values. If $\mathbf{v}_C$ in Figure 5*a* is compared with the solution for $(\mathbf{v}_C+\mathbf{v}_F)$ [not shown], the only major qualitative difference is that $\mathbf{v}_C$ is always directed down-channel, whereas $(\mathbf{v}_C+\mathbf{v}_F)$ is directed up-channel in the vicinity of Barnstaple Bay. The currents $\mathbf{v}_C$ are a compensation for the up-channel directed Stokes drift (see Fig. 1*d*), $\mathbf{v}_S$, and are driven by the set-up of water level due to $\mathbf{v}_S$ (a one-dimensional analysis is given by

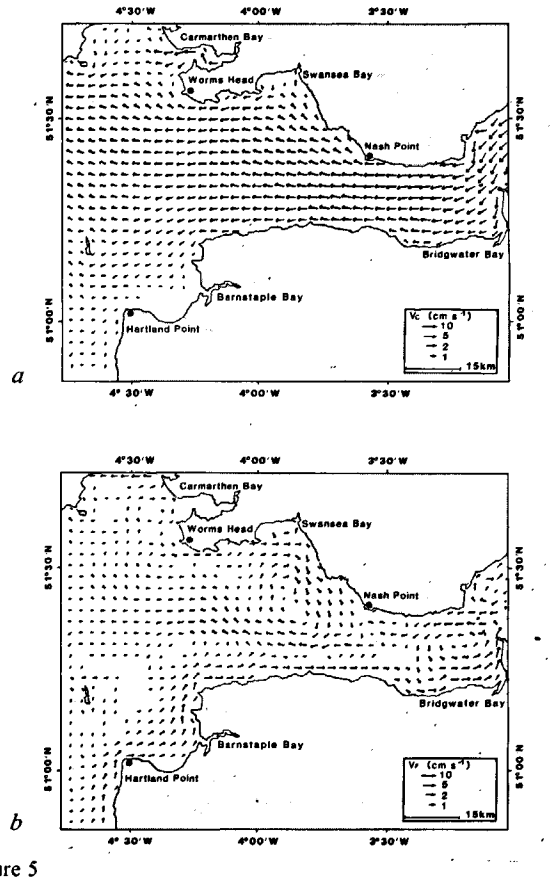

Figure 5

Continuity-driven and frictional-driven residual currents (speeds drawn on a logarithmic scale). Currents with speeds of less than 0.5 mm.sec.$^{-1}$ are not plotted. (a) $\mathbf{v}_C$. (b) $\mathbf{v}_F$.

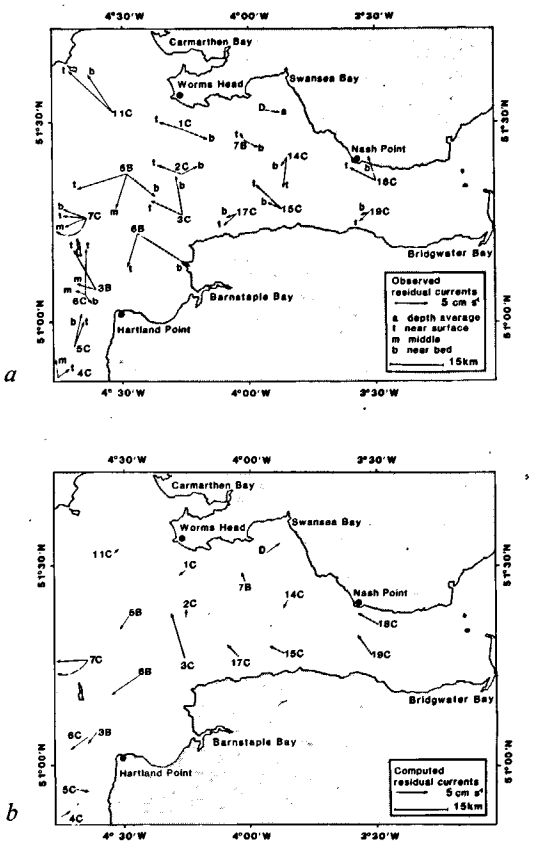

Figure 6

Observed and computed residual currents. (a) Observed currents at near surface (t), middle (m) and near bed (b) current meters. At station D *currents are averaged over the depth. (b) Computed depth averaged residual currents at stations.*

Uncles, Jordan, 1980); as might be anticipated, the set-up is more readily formed in the more enclosed eastern Bristol Channel and Severn Estuary, and is less effective in the open sea area in the south-west of the region, so that the ensuing currents are very weak there.

From the solutions for $\mathbf{v}_F$ given in Figure 5*b* it is clear that the up-channel coastal current in the vicinity of Barnstaple Bay which occurs in the solutions for $(\mathbf{v}_C+\mathbf{v}_F)$ can be attributed to $\mathbf{v}_F$. The forcing mechanism for $\mathbf{v}_F$ is given in equation (13); because $(2u_S-E_{M_4}\cos\varphi_e)>0$ over the region covered it follows that there is an overall forcing into the channel (as with density currents), which manifests itself as up-channel flows in the shallower regions where the forcing is larger, with return flows in the deeper channels. In the region of Barnstaple Bay, Figure 1*d* shows that u_S is much larger here than in the north of the channel, which coupled with shallow depths leads to up-channel flowing currents.

COMPARISON WITH OBSERVATIONS

Observed residual currents are shown in Figure 6*a*, and computed residual currents at the same stations in Figure 6*b*—these being extracted from Figure 2*a*, and as such are representative of $\mathbf{v}_E$ for M_2 tides, and for the salinity distribution shown in Figure 1*b*. With the exception of stations 1 C, 2 C, 3 C and 3 B, for which monthly averaged residual currents are given, these data

correspond to residual currents obtained by averaging over just a few tidal cycles at various states of the spring-neap cycle, and, therefore, can only be compared with computed values in a rather qualitative and subjective way. Currents at station D in Figure 6*a* are averaged over the depth, whereas currents at other stations are given for the near surface (*t*), near bed (*b*), and, where available, the middle (*m*) current meters on each mooring (Uncles and Jordan, in prep.). Data in Figure 6*b* correspond, of course, to depth averaged currents.

If the comparison between observed (imperfect though these generally are) and computed data for the eastern Bristol Channel and Severn Estuary is considered, then stations 18 C, 19 C, 15 C and 17 C in Figure 6*a* show a predominantly down-channel flow at both top and bottom meters, which is also a feature of computed values in Figure 6 *b*. Also, the observed data at stations D and 14 C indicate an anticyclonic coastal current, which is also a feature of computed data.

A comparison is difficult further down-channel owing to the strong rotation of the observed residual currents with depth. Nevertheless, it is apparent that at stations 3 C, 5 B and 6 B the magnitude and direction of the depth averaged currents that one would estimate visually from the observations in Figure 6*a* are in general qualitative accordance with computed data in Figure 6*b*, as are the currents at stations 4 C and 7 C near the seaward boundary. The observed data at stations 5 C, 6 C and 3 B near Hartland Point show a north flowing coastal current, which is also a feature of computed data in Figure 2*a*; that the comparisons between observed and computed data at these stations are poor would appear to be a consequence of the great spatial variability exhibited by the currents in this region, which would further indicate that a finer grid resolution is necessary for their accurate numerical solution. Similarly, the agreement is poor at station 11 C, which may also be a result of large spatial variability in this region and associated numerical errors in the model, or the influence of spring-neap variability in the data.

Vertical structure

The strong rotation with depth of the residual currents shown in Figure 6*a* indicates that depth averaged models can only provide a guide to the true depth averaged currents; this follows from the fact that the residual frictional retardation on a water column is modelled as depending on the depth averaged residual current, whereas in nature it will depend on the current structure near the sea bed, and, for strong rotation of the current vectors, these two frictional effects will be significantly different. However, this inadequacy is mitigated somewhat by the fact that Coriolis forces (the depth averaged values of which are specified in terms of the depth averaged currents) are comparable to frictional forces, and these are modelled accurately.

The generating mechanisms for residual flows also vary in magnitude with depth; thus, the centrifugal forcing term in equation (12) depends on the square of the tidal current, which, in a three-dimensional model, will vary appreciably with depth – especially close to the sea bed. Horizontal density gradients also produce differential forcing through the water column, and it is of interest to investigate whether a significant portion of the observed rotation of the currents with depth can be explained by the density gradients; for this purpose, all other forcing terms are assumed to be constant throughout the water column, so that the depth-dependent linearized equations are (see for example Heaps, 1972):

$$\left.\begin{aligned}\frac{\partial \mathbf{v}_E}{\partial t} = 0 = -\mathbf{f}\times\mathbf{v}_E - g\nabla\zeta^* - gha\nabla S(1-\eta) \\ + \frac{\alpha}{h}\frac{\partial^2 \mathbf{v}_E}{\partial \eta^2},\end{aligned}\right\} \quad (15)$$

with:

$$\frac{\partial \mathbf{v}_E}{\partial \eta} = 0 \quad \text{at } \eta = 1 \quad \text{(the sea surface)}$$

and:

$$\frac{\partial \mathbf{v}_E}{\partial \eta} = \frac{k}{\alpha}\mathbf{v}_E \quad \text{at } \eta = 0 \quad \text{(the sea bed),}$$

in which η is non-dimensional depth, k is a sea bed friction coefficient, and α is the uniform vertical eddy viscosity divided by depth; k and α have been taken as 0.2 and 0.1 cm.sec.$^{-1}$, in accordance with previous modelling work (Heaps, 1972, p. 423). The effective slope, $\nabla\zeta^*$, in equation (15) is assumed to take into account all of the forcing mechanisms except that due to density gradients, and is evaluated by solving equation (15) analytically, averaging the derived currents over the depth, and substituting for these the depth averaged currents from the numerical model.

This procedure has been applied to data from stations 1 C, 2 C and 3 C in Figures 6*a* and *b*, for which monthly averaged values of the residual currents are available, using values of ∇S in equation (15) taken from Figure 1*b*; the results are given in Figure 7, which shows both observed values and those computed from equation (15). The similarity in vertical structure between observed and computed values is striking, and

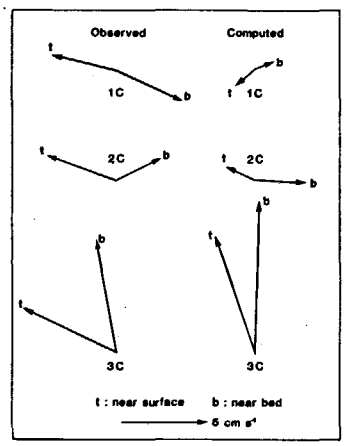

Figure 7
Comparison of observed and computed residual currents at the one-month stations 1 C *to* 3 C, *with allowance in the computed data for vertical variations due to horizontal density gradients.*

demonstrates that density effects can be an important cause of vertical structure in the channel. Naturally, where depth averaged currents are small (as at stations 1C and 2C) the rotation due to density gradients will be pronounced, whereas when they are larger (as at station 3C) the rotation will be small; in general, one would expect the large currents generated near headlands to be little affected by density gradients, and the vertical structure to be determined mainly by the depth variations in centrifugal forcing of the tidal streams.

The existence of significant depth variations in the observed residual currents means that the current patterns displayed in this paper will provide only a guide to the actual depth averaged currents.

CONCLUSIONS

A depth averaged numerical model has been used to evaluate the residual currents generated by horizontal density gradients and M_2 tidal non-linearities in the Bristol Channel; the mechanisms responsible for the generation of these currents have been delineated using a simple linear theory, which clearly shows the formation of currents due to non-linearities in the continuity equation, and those due to density gradients, advection non-linearities, and friction non-linearities in the momentum equation. In general, advection generated currents are largest, followed by those due to continuity and density gradients – currents due to non-linear friction being very small.

The currents generated by continuity non-linearities compensate for the up-channel directed Stokes drift; the Stokes drift produces a set-up in water level, and drives an overall down-channel residual current. The other forcing mechanisms produce residual currents which, in steady-state, have zero net transport over any cross-section of the channel; because the channel is partially enclosed, the forcing must be nearly balanced by surface slopes, which means that currents are driven directly by non-linear or density forcing in sections of the channel where these are strongest, and that the return flows are driven by surface slopes where the forcing mechanisms are small or reversed.

A comparison of the computed depth averaged residual currents with observations shows qualitative similarities at most of the stations, and reasonable agreement for those stations where observations were carried out over one month, and where allowance is made for the expected depth variations due to density gradients.

Acknowledgements

I am grateful to Mr. M. B. Jordan for his assistance with the field observations.

This work, which forms part of the estuarine ecology programme of the Institute for Marine Environmental Research, a component of the Natural Environment Research Council, was partly supported by the Department of the Environment on Contract No. DGR 480/48.

REFERENCES

Bowden K. F., Hamilton P., 1975. Some experiments with a numerical model of circulation and mixing in a tidal estuary, *Estuarine Coastal Mar. Sci.*, **3**, 281-301.

Flather R. A., Heaps N. S., 1975. Tidal computations for Morecambe Bay, *Geophys. J. R. Astron. Soc.*, **42**, 489-517.

Heaps N. S., 1972. Estimation of density currents in the Liverpool Bay area of the Irish Sea, *Geophys. J. R. Astron. Soc.*, **30**, 415-432.

Heaps N. S., 1978. Linearized vertically-integrated equations for residual circulation in coastal seas, *Dtsch. Hydrogr. Z.*, **31**, 147-194.

Hunter J. R., 1975. A note on quadratic friction in the presence of tides, *Estuarine Coastal Mar. Sci.*, **3**, 473-475.

Hunter J. R., 1979. On the interaction of M_2 and $M_{2\,n}$ tidal velocities in relation to quadratic and higher power laws, *Dtsch. Hydrogr. Z.*, **32**, 146-153.

Miles G. V., 1979. Estuarine modelling – Bristol Channel, in: *Tidal power and estuary management*, edited by R. T. Severn *et al.*, Scientechnica, 76-84.

Nihoul J. C., Ronday F. C., 1975. The influence of tidal stress on the residual circulation, *Tellus*, **27**, 484-489.

Oonishi Y., 1977. A numerical study on the tidal residual flow, *J. Oceanogr. Soc. Jpn*, **33**, 207-218.

Oonishi Y., 1978. A numerical study on the tidal residual flow-vertical motion induced by tidal current, *J. Oceanogr. Soc. Jpn*, **34**, 140-159.

Owen A., 1980. The tidal regime of the Bristol Channel: a numerical modelling approach, *Geophys. J. R. Astron. Soc.*, **62**, 59-75.

Pingree R. D., 1978. The formation of the Shambles and other banks by tidal stirring of the seas, *J. Mar. Biol. Assoc. U.K.*, **58**, 211-226.

Pingree R. D., Maddock L., 1977. Tidal residuals in the English Channel, *J. Mar. Biol. Assoc. U.K.*, **57**, 339-354.

Prandle D., 1978. Residual flows and elevations in the Southern North Sea, *Proc. R. Soc. London, ser. A*, **359**, 189-228.

Tee K. T., 1976. Tide-induced residual current, a 2-d non-linear numerical tidal model, *J. Mar. Res.*, **34**, 603-628.

Tee K. T., 1977. Tide-induced residual current – verification of a numerical model, *J. Phys. Oceanogr.*, **7**, 396-402.

Uncles R. J., 1981. A note on tidal asymmetry in the Severn Estuary, *Estuarine Coastal Shelf Sci.*, **13**, 419-432.

Uncles R. J., Jordan M. B., 1980. A one-dimensional representation of residual currents in the Severn Estuary and associated observations, *Estuarine Coastal Mar. Sci.*, **10**, 39-60.

Yanagi T., 1976. Fundamental study on the tidal residual circulation-1, *J. Oceanogr. Soc. Jpn*, **32**, 199-208.

Yanagi T., 1977. Tidal residual flow in Kasado Bay, *J. Oceanogr. Soc. Jpn*, **33**, 335-339.

Yanagi T., 1978. Fundamental study on the tidal residual circulation, 2, *J. Oceanogr. Soc. Jpn*, **34**, 67-72.

Zimmerman J. T. F., 1978. Topographic generation of residual circulation by oscillatory (tidal) currents, *Geophys. Astrophys. Fluid Dynamics*, **11**, 35-47.

APPENDIX

In the absence of knowledge on the distributions of ζ_E, ζ_D, ζ_A, ζ_F and ζ_C along the seaward boundary, an obvious assumption to make is that each is zero; therefore, distributions of the dominant residual currents in the western Bristol Channel, $\mathbf{v}_E$, $\mathbf{v}_A$ and $\mathbf{v}_D$ (see Table), were computed using this assumption as a means of testing the sensitivity of the solutions to vagueness in the seaward boundary conditions.

In the case of residual variables, it might be anticipated that the effects of poorly prescribed seaward boundary conditions will become weaker progressing further into the domain, away from the boundary. To verify this, the residual currents generated solely by boundary elevations were investigated for the case where a uniform

surface slope exists along the seaward boundary, leading to a 1 cm increase in water level from south to north coastlines. Currents in the western Bristol Channel decreased rapidly (exponentially) away from the boundary, so that those in the eastern Bristol Channel and Severn Estuary were negligible.

As mentioned, values of ζ_D used to derive $\mathbf{v}_D$ in Figure 3*a* were estimated by balancing surface slope and density gradient forcing along the seaward boundary, leading to a 2 cm increase in water level from south to north coastlines. This balance must be very nearly the real situation, and is certainly much more realistic than assuming $\zeta_D = 0$ along the seaward boundary; nevertheless, when the distribution of $\mathbf{v}_D$ obtained using this assumption is compared with Figure 3*a*, then the effects of these different boundary conditions are only evident in the most western part of the Channel ($\sim$12 km from the boundary).

The tidally-induced residual elevations along the seaward boundary have been estimated from a coarse-grid model of the southwest shelf—as previously described; adding ζ_D to these elevations provides boundary values for ζ_E which were used to determine $\mathbf{v}_E$ in Figure 2*a*. If residual currents, $\mathbf{v}_E$, computed using $\zeta_E = 0$ along the seaward boundary are compared with Figure 2*a*, then the effects of these different boundary conditions are again only evident in the most western part of the Channel ($\sim$9 km from the boundary). The same result follows from solving $\mathbf{v}_A$ with $\zeta_A = 0$ along the seaward boundary and comparing with Figure 4*a*.

It seems reasonable to conclude that poorly prescribed boundary elevations will only have a significant effect on the residual currents in the most western part of the domain studied. Important differences exist between computed and observed residual currents at stations 5 C, 6 C, 3 B and 11 C near the seaward boundary in Figures 6*a* and *b*; however, computed residual currents at these stations, derived using $\zeta_E = 0$ at the seaward boundary, are not significantly different from those plotted in Figure 6*b*. Therefore, differences between observed and computed currents at these stations are unlikely to be a consequence of poor boundary conditions.